Supporting Information

for

Di-functional Luminescent Sensors Based on Y^{3+} Doped Eu^{3+} and Tb^{3+} Coordination Polymers: Fast Responsive and Visible Detection of Cr^{3+}, Fe^{3+} ions in aqueous solutions and Acetone

Hongyan Liu, [a] Yang Liu, [a] Yu Meng, [a] Xiaolei Shi,[a] Junshan Sun,[b] Limin Zhao,[a] Diming Chen,[c] Hongguo Hao,*[a] Dacheng Li,*[a] Jianmin Dou ,[a] and Jun Han [d]

[a]*Shandong Provincial Key Laboratory of Chemical Energy Storage and Novel Cell Technology, School of Chemistry and Chemical Engineering, College of Materials Science and Engineering, Institute of Biopharmaceutical Research, Liaocheng University, Liaocheng 252059, People's Republic of China*

E-mail:hhg207@126.com, lidacheng62@163.com.

[b]*College of Chemistry and Chemical Engineering, Taishan University, Taian 271000, Shandong Province, People's Republic of China*

[c]*School of Computer and Communication Engineering, Zhengzhou University of Light Industry, Zhengzhou 450002, People's Republic of China*

Table S1

Complex	**1-Y**	**1-Eu**[1]	**1-Tb**[1]	**1-Gd**[2]
Crystal data	1989014	1814159	1814160	1864276
formula	$[Y(C_{16}H_6O_8)_{0.5}(C_4H_9ON)(C_2H_3O_2)(H_2O)]$	$[Eu_2(C_{16}H_6O_8)(C_4H_6ON)_2(C_2H_3O_2)_2]\cdot 4H_2O$	$[Tb_2(C_{16}H_6O_8)(C_4H_6ON)_2(C_2H_3O_2)_2]\cdot 4H_2O$	$[Gd(C_{16}H_6O_8)_{0.5}(C_4H_9ON)(C_2H_3O_2)(H_2O)]$
M_r	416.2	988.5	1002.4	484.5
Temperature/K	298	298	298	298
crystal size/mm^3	0.11 × 0.14 × 0.14	0.13 × 0.16 × 0.14	0.13 × 0.12 × 0.15	0.11 × 0.15 × 0.13
Crystal system,	Monoclinic	Monoclinic	Monoclinic	Monoclinic
space group	$P2_1/n$	$P2_1/n$	$P2_1/n$	$P2_1/n$
a (Å)	9.3026(8)	9.4453(5)	9.3676(7)	9.3992(8)
b (Å)	17.5625 (14)	17.7439(14)	17.6232(14)	17.6714(15)
c (Å)	11.3369 (9)	11.3019(8)	11.3172(9)	11.2971(9)
α, β, γ/°	90, 94.35(1), 90	90, 94.278(1), 90	90, 94.351(2), 90	90, 94.318(3), 90
V/Å^3	1846.9(3)	1888.9(2)	1862.9(3)	1871.1(3)
Z	2	1	1	2
F(000)	836	932	972	944
Radiation type	Mo *Kα*	Mo *Kα*	Mo *Kα*	Mo *Kα*
μ (mm^{-1})	3.2	3.36	3.83	3.58
Data collection	Bruker APEXII CCD	Bruker APEXII CCD	Bruker APEXII CCD	Bruker APEXII CCD
Diffractometer	Multi-scan (SADABS;	Multi-scan (SADABS;	Multi-scan (SADABS;	Multi-scan (SADABS;
Absorption correction	Sheldrick, 2003)	Sheldrick, 2003)	Sheldrick, 2003)	Sheldrick, 2003)
T_{min}, T_{max}	0.682, 0.741	0.356, 0.610	0.659, 0.656	0.368, 0.423
No. of measured, independent and observed [$I > 2\sigma(I)$] reflections	3254, 3254, 1686	8950, 3206, 2250	8955, 3162, 2200	8879, 3296, 2207
R_{int}	0.060	0.0101	0.072	0.0080
$(\sin\theta/\lambda)_{max}$ (Å^{-1})	0.595	0.595	0.595	0.595
Refinement $R[F^2 > 2\sigma(F^2)]$, $wR(F^2)$, *S*	0.062, 0.294,1.0	0.072,0.196,0.96	0.060,0.155,1.01	0.091,0.258,1.07
No. of reflections	3354	3206	3162	3296
No. of parameters	222	208	221	209
H-atom treatment	H-atom parameters constrained	H-atom parameters constrained	H-atom parameters constrained	H-atom parameters constrained
$\Delta\rho_{max}$, $\Delta\rho_{min}$	1.80, -1.00	1.42, -2.36	1.50, -1.58	2.43, -2.74

Computer programs: *CrysAlis PRO*, Agilent Technologies, *SHELXL97* (Sheldrick, 1997). *SHELXL*2014 (Sheldrick, 2015), *DIAMOND* (Brandenburg & Putz, 2005) *and publCIF* (Westrip, 2010).

1-Eu, **1-Tb** and **1-Gd** have been published in our previous work.[1-2]

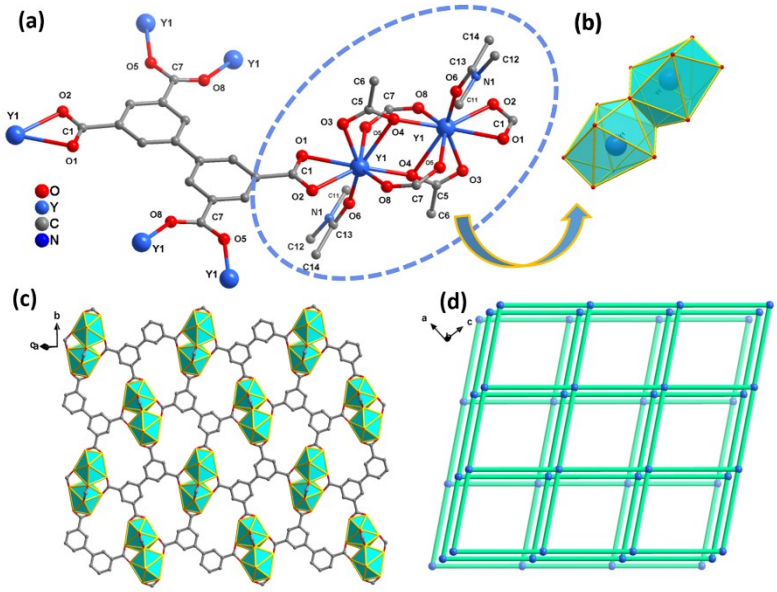

Fig.S1 View of the coordination environments of the ligand (a) and Y(Ⅲ)(b) atoms. (code: C, gray ; O, red; N, dark blue; Y, blue) The hydrogen atoms are omitted for clarity. (c) The polyhedron of 3D framework viewed from b axis. (d) The simplified topology structure of **1-Y**.

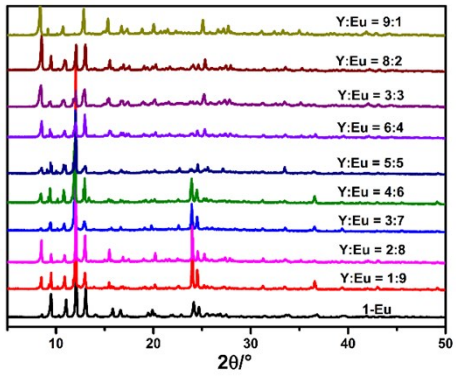

Fig. S2 PXRD patterns of $\mathbf{Eu_xY_{1-x}}$ (x = 0.1, 0.2, 0.3, 0.4, 0.5, 0.6, 0.7, 0.8, 0.9).

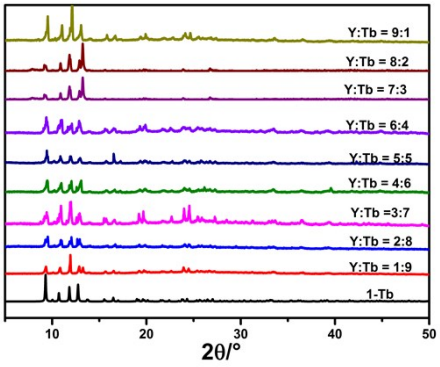

Fig.S3 PXRD patterns of $\mathbf{Tb_xY_{1-x}}$ (x = 0.1, 0.2, 0.3, 0.4, 0.5, 0.6, 0.7, 0.8, 0.9).

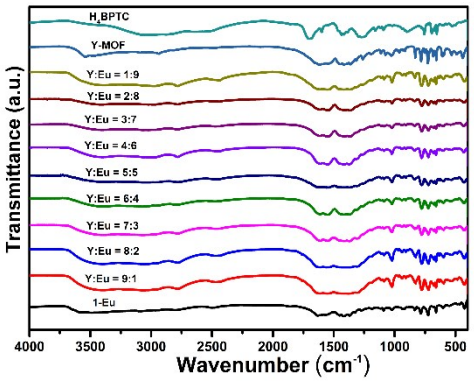

Fig.S4 IR spectra (KBr pellet, cm^{-1}) of H_4BPTC, **1-Y** and $\mathbf{Eu_xY_{1-x}}$ (x = 0.1, 0.2, 0.3, 0.4, 0.5, 0.6, 0.7, 0.8, 0.9).

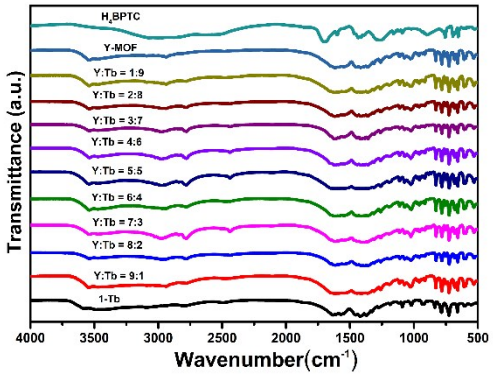

Fig.S5 IR spectra (KBr pellet, cm^{-1}) of H_4BPTC, **1-Y** and $\mathbf{Tb_xY_{1-x}}$ (x = 0.1, 0.2, 0.3, 0.4, 0.5, 0.6, 0.7, 0.8, 0.9).

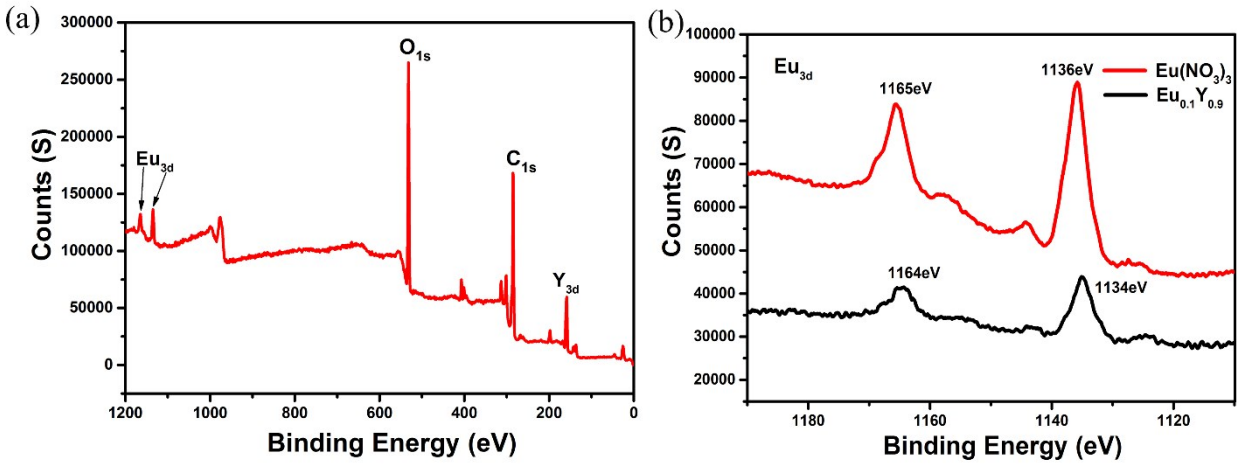

Fig. S6 XPS spectra (a) and (b) Eu3d of $\mathbf{Eu_xY_{1-x}}$.

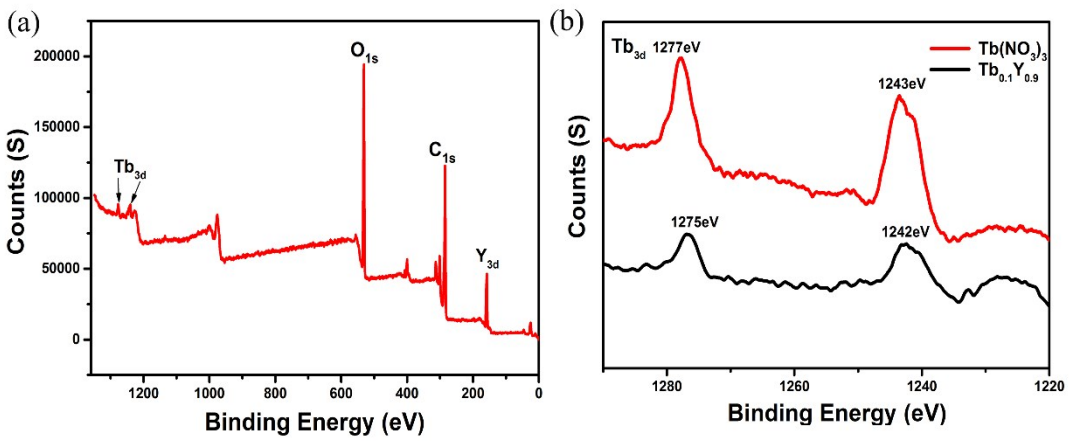

Fig. S7 XPS spectra (a) and (b) Tb3d of $\mathbf{Tb_xY_{1-x}}$.

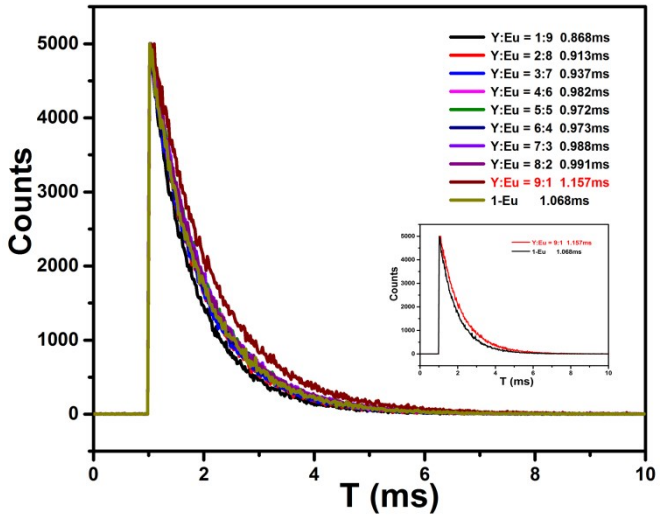

Fig.S8 The luminescence decay lifetimes of $\mathbf{Eu_xY_{1-x}}$ at room temperature. Insert: The luminescence decay lifetimes of **1-Eu** and $\mathbf{Eu_{0.1}Y_{0.9}}$.

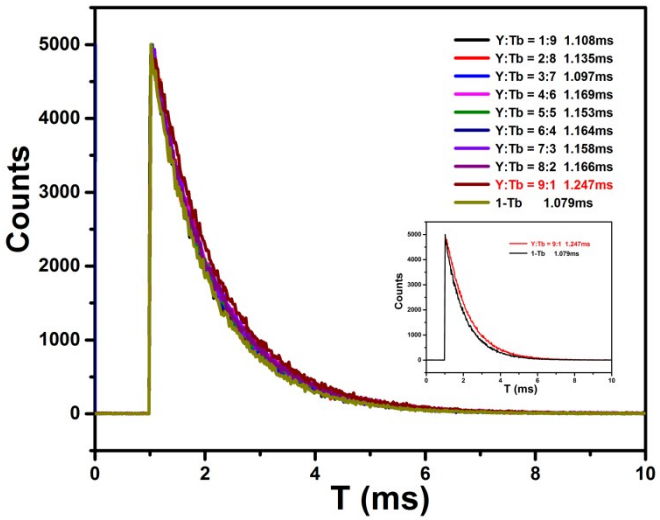

Fig.S9 The luminescence decay lifetimes of $\mathbf{Tb_xY_{1-x}}$ at room temperature. Insert: The luminescence decay lifetimes of **1-Tb** and $\mathbf{Tb_{0.1}Y_{0.9}}$.

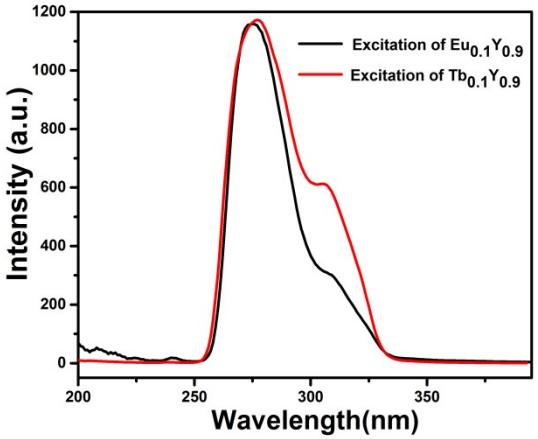

Fig. S10 The excitation spectra of $\mathbf{Eu_{0.1}Y_{0.9}}$ and $\mathbf{Tb_{0.1}Y_{0.9}}$.

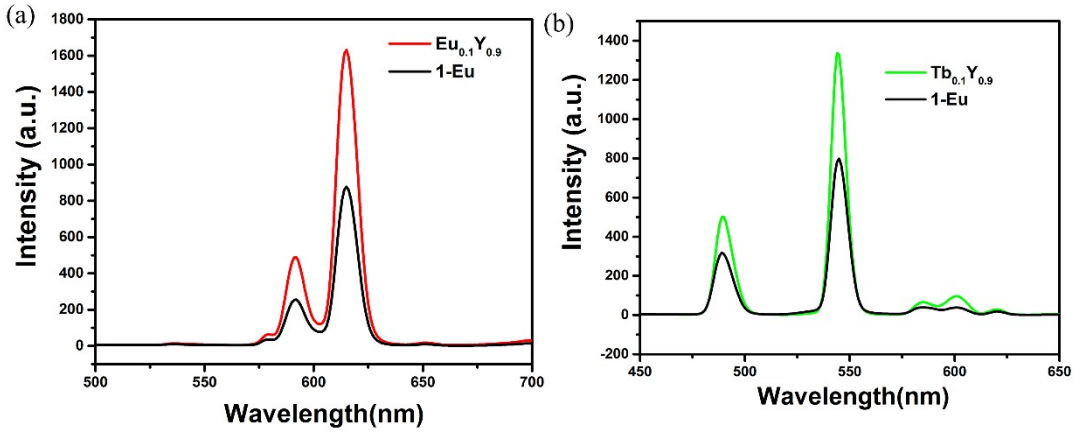

Fig.S11 Luminescent spectra of (a) $\mathbf{Eu_{0.1}Y_{0.9}}$, **1-Eu** and (b) $\mathbf{Tb_{0.1}Y_{0.9}}$, **1-Tb** (2mg) in DMF (2mL) when excited at 275 nm.

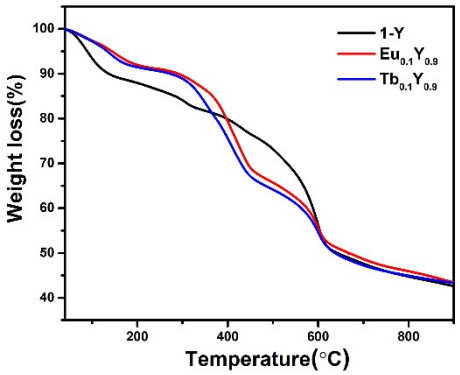

Fig.S12 TG curves of **1-Y**, $\mathbf{Eu_{0.1}Y_{0.9}}$ and $\mathbf{Tb_{0.1}Y_{0.9}}$.

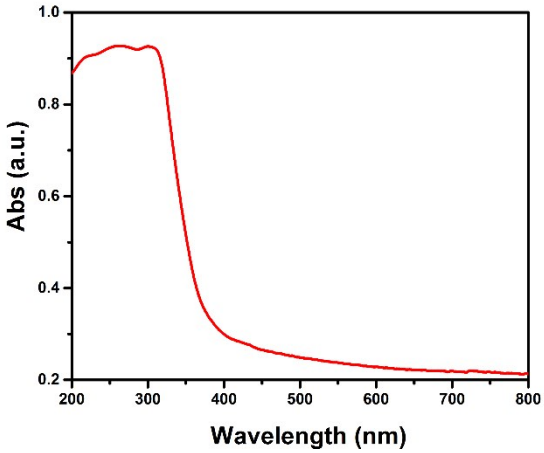

Fig.S13 UV-vis adsorption spectra of H_4BPTC in the solid state at room temperature.

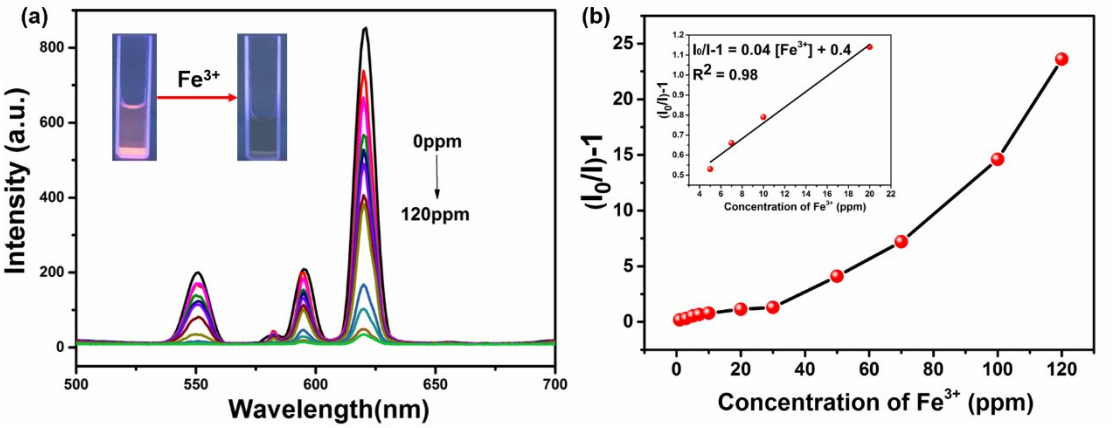

Fig.S14 (a) Luminescent spectra of $\mathbf{Eu_{0.1}Y_{0.9}}$ upon the addition of various Fe^{3+} concentrations in DMF when excited at 275 nm. (b) Nonlinear Stern-Volmer plot for Fe^{3+} by exponential quenching equation. Inset: linear fitting plot of the Stern-Volmer plot with 0-20 ppm of Fe^{3+}.

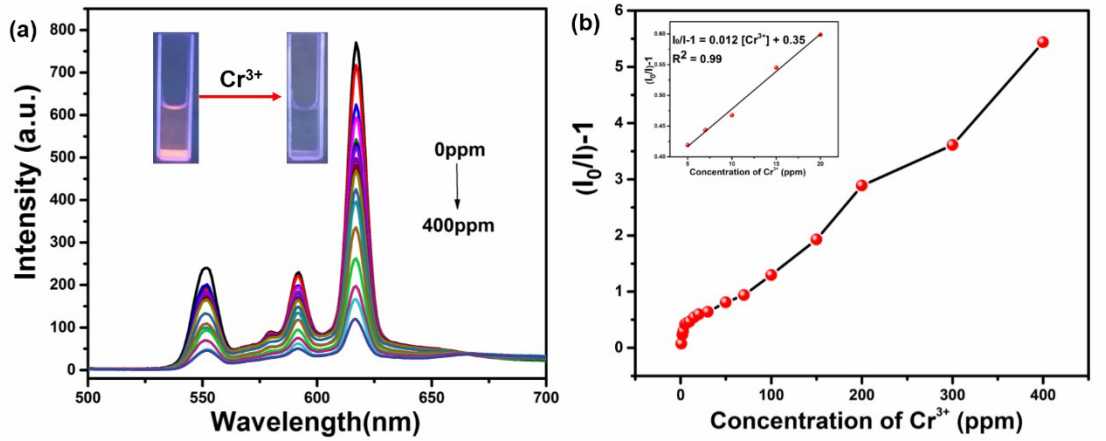

Fig.S15 (a) Luminescent spectra of $\mathbf{Eu_{0.1}Y_{0.9}}$ upon the addition of various Cr^{3+} concentrations in DMF when excited at 275 nm. (b) Nonlinear Stern-Volmer plot for

Cr^{3+} by exponential quenching equation. Inset: linear fitting plot of the Stern-Volmer plot with 0-20 ppm of Cr^{3+}.

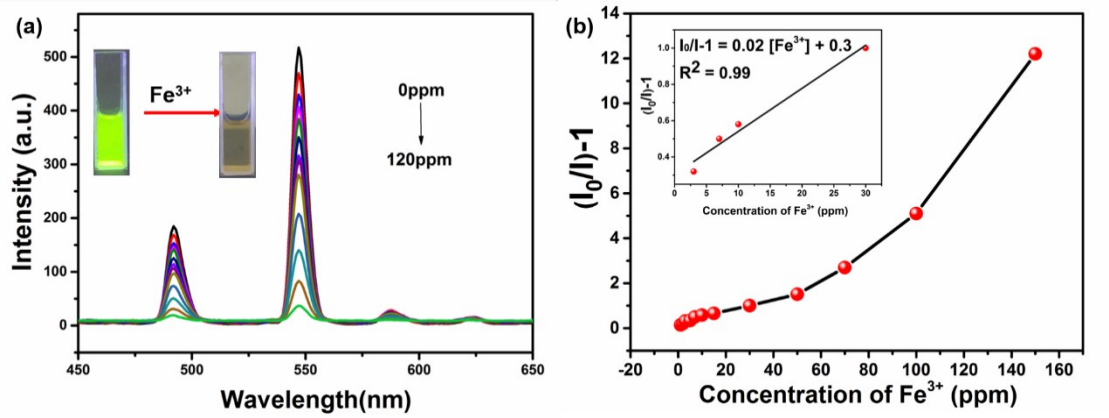

Fig.S16 (a) Luminescent spectra of $\mathbf{Tb_{0.1}Y_{0.9}}$ upon the addition of various Fe^{3+} concentrations in DMF when excited at 275 nm. (b) Nonlinear Stern-Volmer plot for Fe^{3+} by exponential quenching equation. Inset: linear fitting plot of the Stern-Volmer plot with 0-30 ppm of Fe^{3+}.

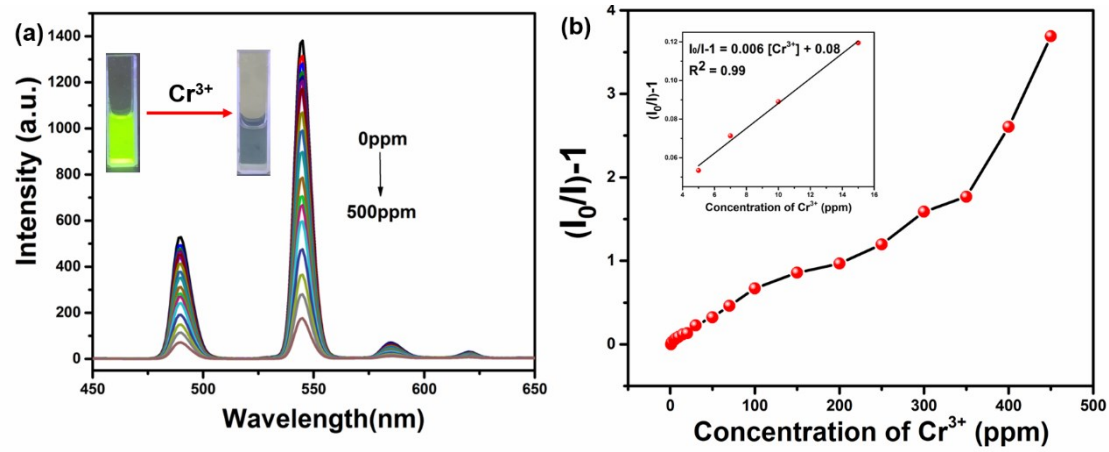

Fig.S17 (a) Luminescent spectra of $\mathbf{Tb_{0.1}Y_{0.9}}$ upon the addition of various Cr^{3+} concentration in DMF when excited at 275 nm. (b) Nonlinear Stern-Volmer plot for Cr^{3+} by exponential quenching equation. Inset: linear fitting plot of the Stern-Volmer plot with 0-15 ppm of Cr^{3+}.

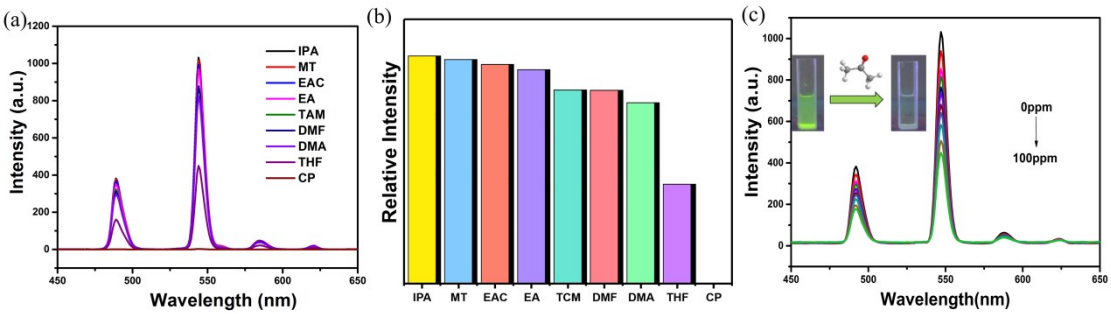

Fig.S18 (a) Luminescent spectra of $\mathbf{Tb_{0.1}Y_{0.9}}$ dissolved in different solvents (λex = 275 nm). (b) Bar chart obtained for $\mathbf{Tb_{0.1}Y_{0.9}}$ upon addition of different solvents. (c) Luminescent spectra of $\mathbf{Tb_{0.1}Y_{0.9}}$ with the gradual addition of acetone (0-100ppm).

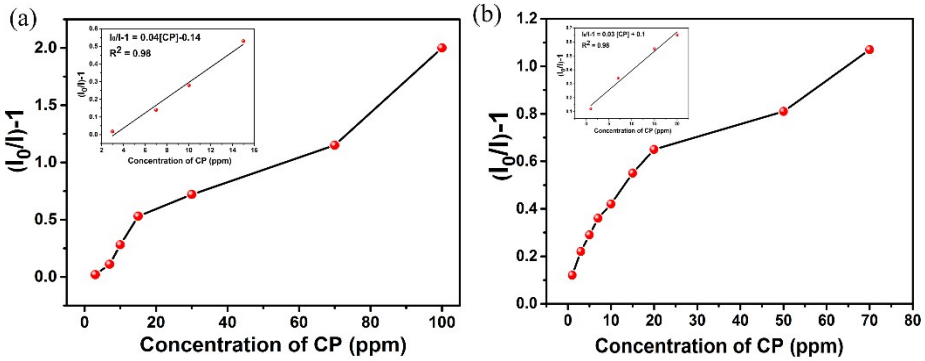

Fig.S19 (a) Nonlinear Stern-Volmer plot for acetone by exponential quenching equation for $\mathbf{Eu_{0.1}Y_{0.9}}$. Inset: linear fitting plot of the Stern-Volmer plot with 0-15 ppm of acetone. (b) Nonlinear Stern-Volmer plot for acetone by exponential quenching equation for $\mathbf{Tb_{0.1}Y_{0.9}}$. Inset: linear fitting plot of the Stern-Volmer plot with 0-20 ppm of acetone.

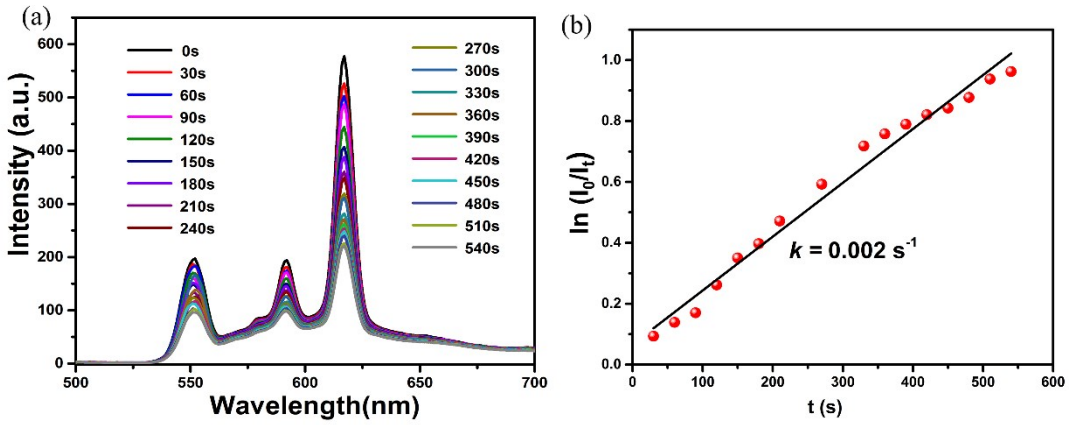

Fig.S20 (a) Time-dependent emission spectra after exposure of $\mathbf{Eu_{0.1}Y_{0.9}}$ to Cr^{3+} (λ_{ex} = 275 nm). (b) Plots of ln (I_0/I_t) for the luminescent intensity of $\mathbf{Eu_{0.1}Y_{0.9}}$ at 615 nm obtained from the spectra.

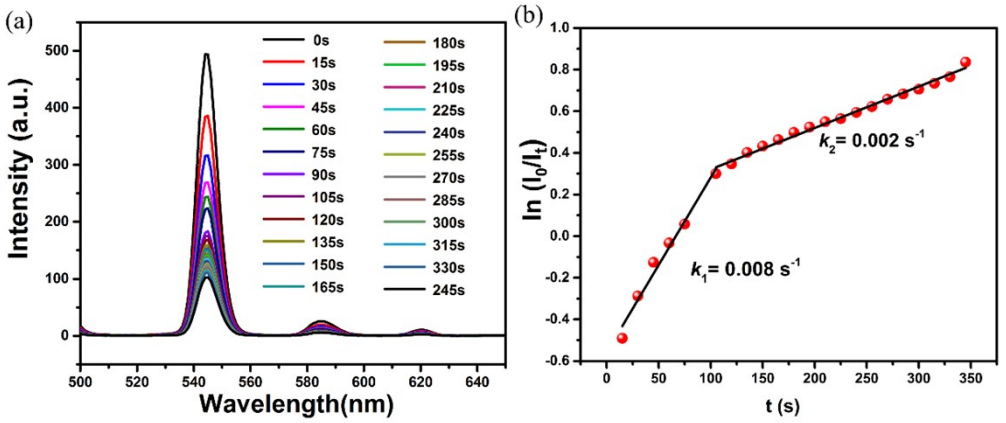

Fig.S21 (a) Time-dependent emission spectra after exposure of $\mathbf{Tb_{0.1}Y_{0.9}}$ to Fe^{3+} (λ_{ex} = 275 nm). (b) Plots of ln (I_0/I_t) for the luminescent intensity of $\mathbf{Tb_{0.1}Y_{0.9}}$ at 544 nm obtained from the spectra.

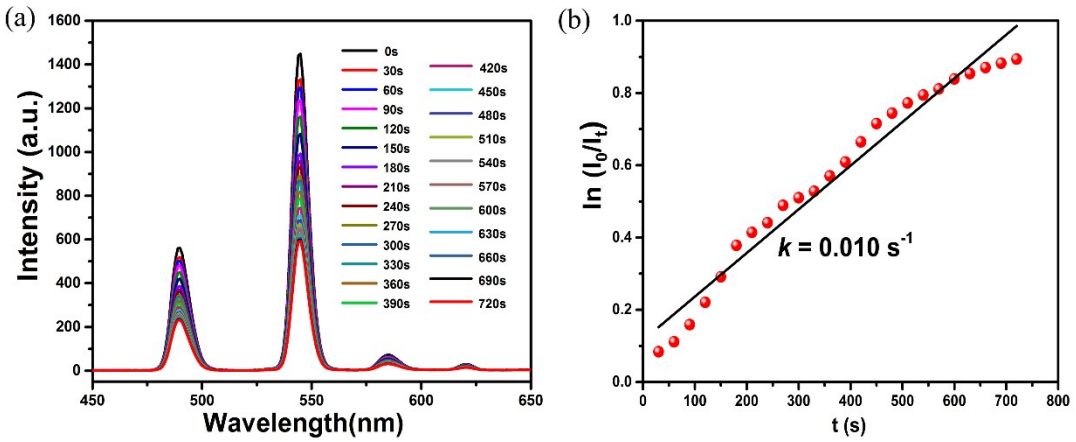

Fig.S22 (a) Time-dependent emission spectra after exposure of $\mathbf{Tb_{0.1}Y_{0.9}}$ to Cr^{3+} (λ_{ex} = 275 nm). (b) Plots of ln (I_0/I_t) for the luminescent intensity of $\mathbf{Tb_{0.1}Y_{0.9}}$ at 544 nm obtained from the spectra.

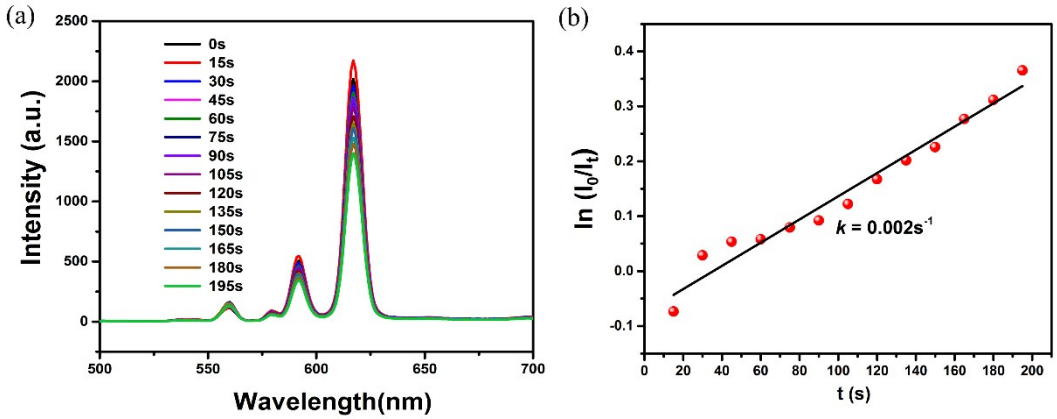

Fig.S23 (a) Time-dependent emission spectra after exposure of **1-Eu** to Fe^{3+} (λ_{ex} = 275 nm). (b) Plots of ln (I_0/I_t) for the luminescent intensity of **1-Eu** at 615nm obtained from the spectra.

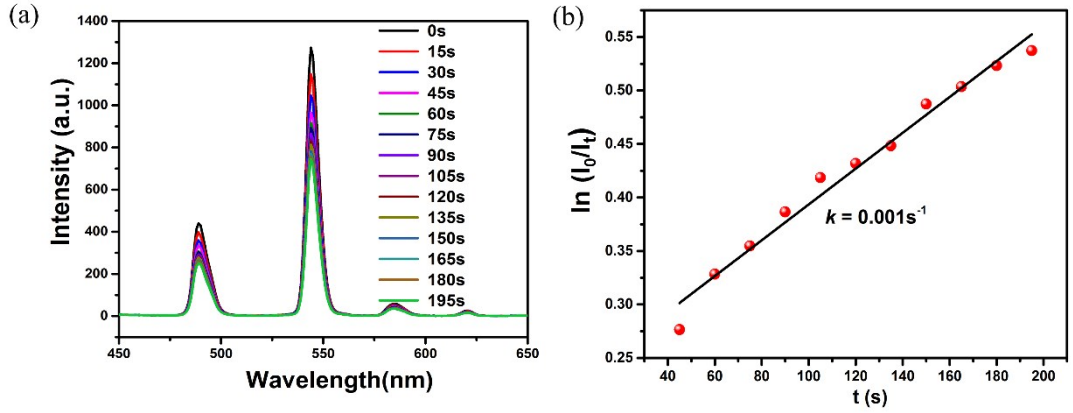

Fig.S24 (a) Time-dependent emission spectra after exposure of **1-Tb** to Fe^{3+} (λ_{ex} = 275 nm). (b) Plots of ln (I_0/I_t) for the luminescent intensity of **1-Tb** at 544 nm obtained from the spectra.

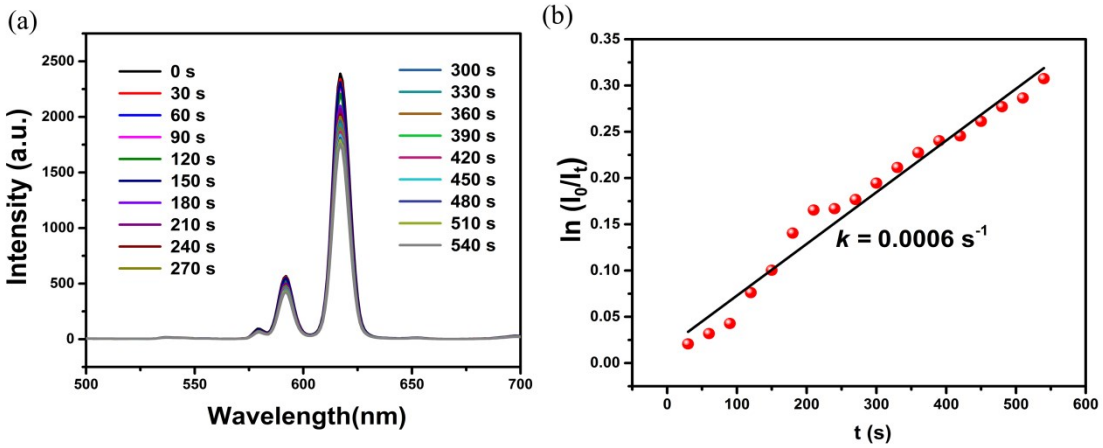

Fig.S25 (a) Time-dependent emission spectra after exposure of **1-Eu** to Cr^{3+} (λ_{ex} = 275 nm). (b) Plots of ln (I_0/I_t) for the luminescent intensity of **1-Eu** at 615nm obtained from the spectra.

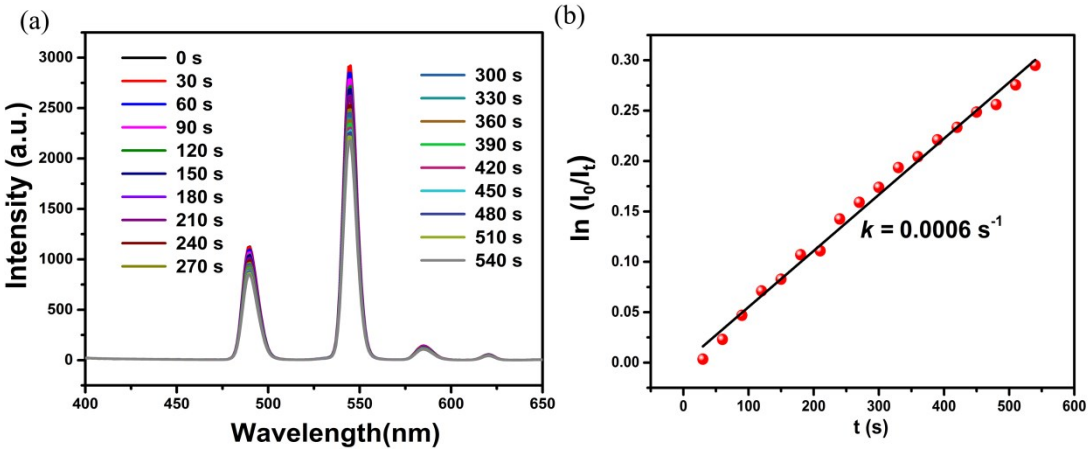

Fig.S26 (a) Time-dependent emission spectra after exposure of **1-Tb** to Cr^{3+} (λ_{ex} = 275 nm). (b) Plots of ln (I_0/I_t) for the luminescent intensity of **1-Tb** at 544nm obtained from the spectra.

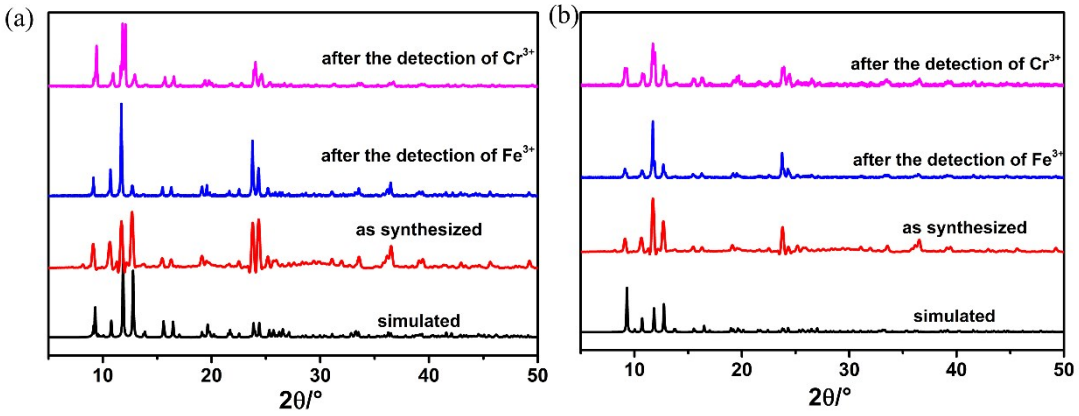

Fig.S27 The PXRD pattern of (a) $\mathbf{Eu_{0.1}Y_{0.9}}$ and (b) $\mathbf{Tb_{0.1}Y_{0.9}}$ before and after the detection of Fe^{3+}, $Cr^{3+}$and acetone.

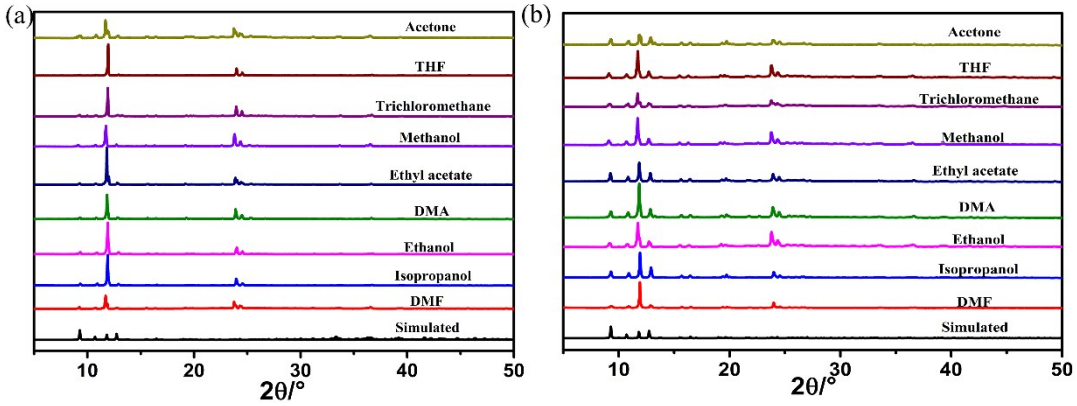

Fig.S28 PXRD patterns of (a) $\mathbf{Eu_{0.1}Y_{0.9}}$ and (b) $\mathbf{Tb_{0.1}Y_{0.9}}$ immersed in different organic solutions for 24 hours.

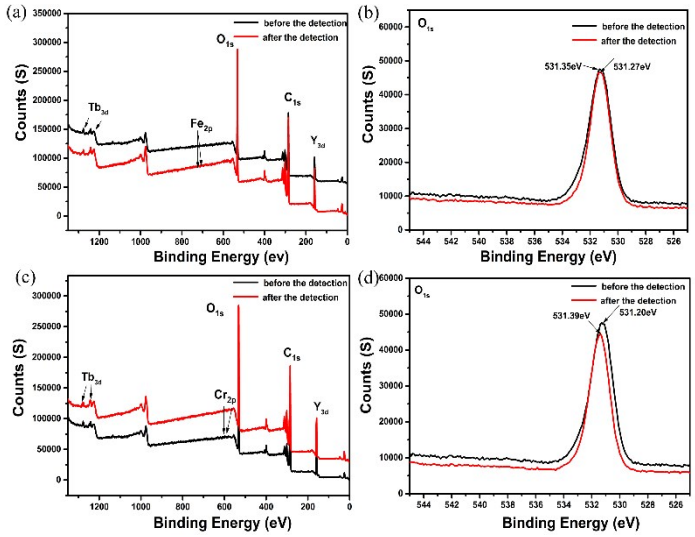

Fig.S29 The XPS spectra of $\mathbf{Tb_{0.1}Y_{0.9}}$ before and after the detection of Fe^{3+} and Cr^{3+}.

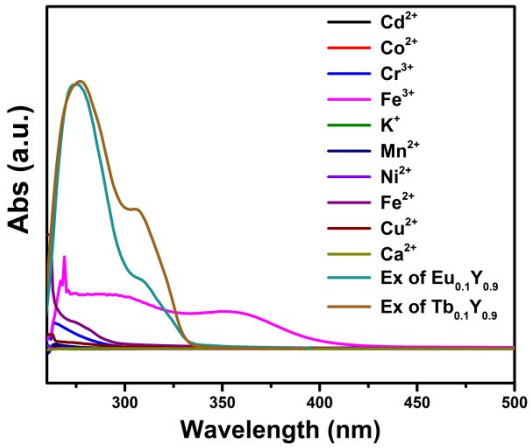

Fig.S30 Spectral overlap between the excitation spectrum of $\mathbf{Eu_{0.1}Y_{0.9}}$, $\mathbf{Tb_{0.1}Y_{0.9}}$ (λ_{ex} = 275 nm) and the absorption spectra of metal ions investigated in this work.

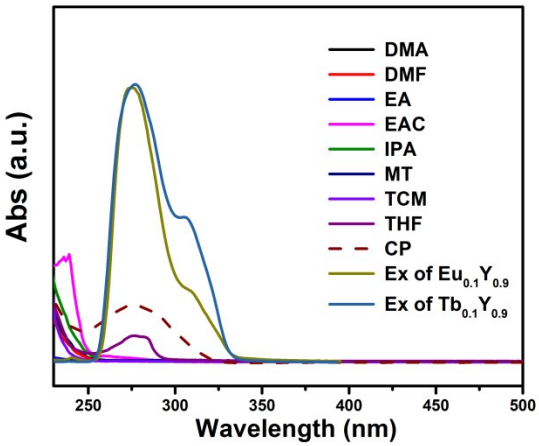

Fig.S31 Spectral overlap between the excitation spectrum of $\mathbf{Eu_{0.1}Y_{0.9}}$, $\mathbf{Tb_{0.1}Y_{0.9}}$ (λ_{ex} = 275 nm) and the absorption spectra of organic solutions investigated in this work.

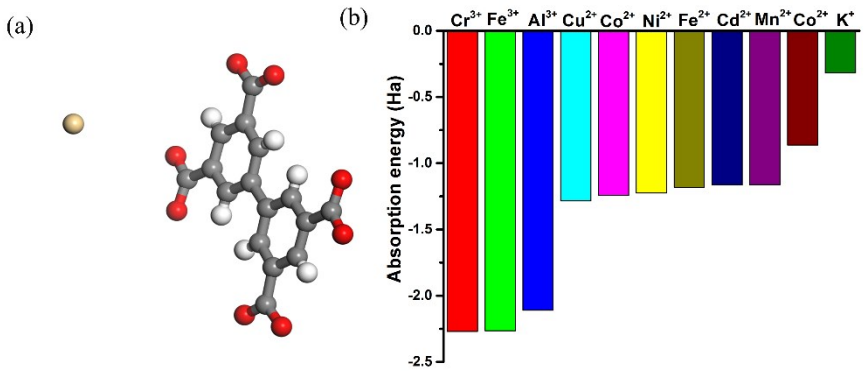

Fig. S32 (a) The proposed structural model of M^{n+} in 1-Ln. (code: C, gray; O, red; M^{n+}, brown). (b) The adsorption energy results of 1-Ln treated with different metal ions calculated by DFT.

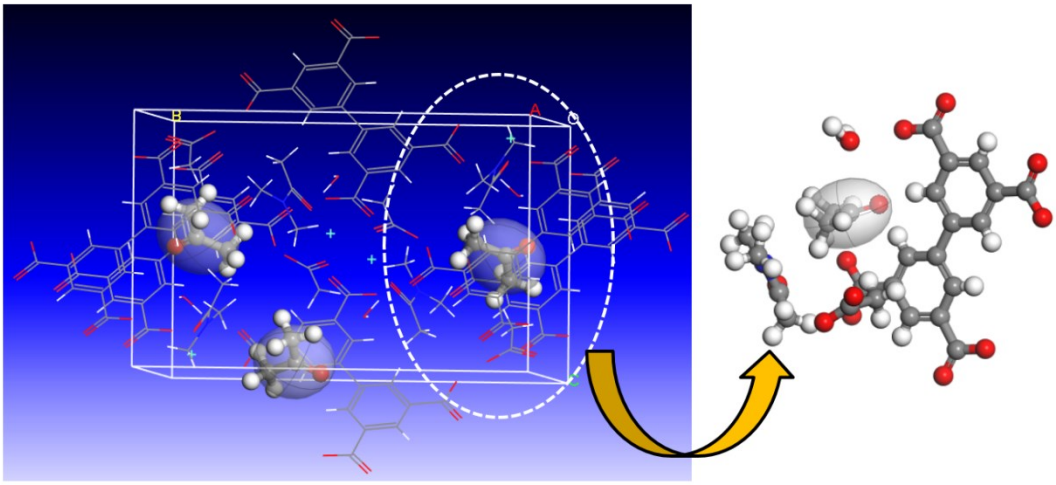

Fig.S33 The calculated adsorption locate for acetone in 1-Ln using the Sorption method.

Table S2

CP	Metal ratios from starting material preparation	Metal ratios from ICP of digested sample	X
$Eu_{0.9}Y_{0.1}$ x = 0.9	Eu : Y = 9 : 1	Eu : Y = 0.91 : 0.09	0.91
$Eu_{0.8}Y_{0.2}$ x = 0.8	Eu : Y = 8 : 2	Eu : Y = 0.82 : 0. 18	0.82
$Eu_{0.6}Y_{0.4}$ x = 0.6	Eu : Y = 6 : 4	Eu : Y = 0.64 : 0.36	0.64
$Eu_{0.5}Y_{0.5}$ x = 0.5	Eu : Y = 5 : 5	Eu : Y = 0.53: 0.57	0.53
$Eu_{0.3}Y_{0.7}$ x = 0.3	Eu : Y = 3 : 7	Eu : Y = 0.29 : 0.71	0.29
$Eu_{0.2}Y_{0.8}$ x = 0.2	Eu : Y =2 : 8	Eu : Y = 0.24 : 0.76	0.24
$Eu_{0.1}Y_{0.9}$ x = 0.1	Eu : Y = 1 : 9	Eu : Y = 0.08 : 0.92	0.08

CP	Metal ratios from starting material preparation	Metal ratios from ICP of digested sample	X

$Tb_{0.8}Y_{0.2}$ x = 0.8	Tb : Y = 8 : 2	Tb: Y = 0. 87: 0. 13	0.87
$Tb_{0.6}Y_{0.4}$ x = 0.6	Tb : Y = 6 : 4	Tb: Y = 0.67 : 0.33	0.67
$Tb_{0.4}Y_{0.6}$ x = 0.4	Tb : Y = 4 : 6	Tb: Y = 0.33 : 0.64	0.33
$Tb_{0.2}Y_{0.8}$ x = 0.2	Tb: Y =2 : 8	Tb : Y = 0.21 : 0.79	0.21
$Tb_{0.1}Y_{0.9}$ x = 0.1	Tb : Y = 1 : 9	Tb: Y = 0.19 : 0.81	0.19

Table S3 Quantum yield of Eu_xY_{1-x} and Tb_xY_{1-x}.

Sample	Quantum yield (Φ)	Sample	Quantum yield (Φ)
$Eu_{0.9}Y_{0.1}$	45.35%	$Tb_{0.9}Y_{0.1}$	24.81%
$Eu_{0.8}Y_{0.2}$	59.57%	$Tb_{0.8}Y_{0.2}$	18.88%
$Eu_{0.7}Y_{0.3}$	65.66%	$Tb_{0.7}Y_{0.3}$	23.47%
$Eu_{0.6}Y_{0.4}$	70.53%	$Tb_{0.6}Y_{0.4}$	26.51%
$Eu_{0.5}Y_{0.5}$	74.47%	$Tb_{0.5}Y_{0.5}$	22.26%
$Eu_{0.4}Y_{0.6}$	73.19%	$Tb_{0.4}Y_{0.6}$	19.39%
$Eu_{0.3}Y_{0.7}$	71.41%	$Tb_{0.3}Y_{0.7}$	17.99%
$Eu_{0.2}Y_{0.8}$	66.73%	$Tb_{0.2}Y_{0.8}$	15.45%
$Eu_{0.1}Y_{0.9}$	69.04%	$Tb_{0.1}Y_{0.9}$	14.02%
1-Eu	62.65%	1-Tb	20.32%

Table S4 Selected bond lengths (Å) for **1-Y**.

Atom	Atom	Length/Å	Atom	Atom	Length/Å
Y1	O2	2.397(8)	Y1	O3	2.397(11)
Y1	O6	2.211(13)	Y1	O1	2.457(9)
Y1	O5	2.294(9)	Y1	O4	2.561(9)
Y1	$O4^1$	2.303(9)			

Table S5 Selected bond angles (°) for **1-Y**.

Atom	Atom	Atom	Angle/°	Atom	Atom	Atom	Angle/°
O6	Y1	O5	89.2(7)	O6	Y1	O1	76.5(5)
O6	Y1	$O4^1$	80.1(4)	O5	Y1	O1	78.8(3)
O5	Y1	O4	76.2(3)	$O4^1$	Y1	O1	145.8(3)
O6	Y1	$O8^1$	116.2(7)	$O8^1$	Y1	O1	135.8(3)
O5	Y1	$O8^1$	139.1(3)	O3	Y1	O1	75.2(4)
$O4^1$	Y1	$O8^1$	77.3(3)	O2	Y1	O1	53.9(3)
O6	Y1	O3	151.6(5)	O6	Y1	O4	150.5(5)
O5	Y1	O3	87.1(4)	O5	Y1	O4	70.0(3)
$O4^1$	Y1	O3	126.0(4)	$O4^1$	Y1	O4	74.8(3)
$O8^1$	Y1	O3	83.8(4)	O9	Y1	O4	85.7(3)
O6	Y1	O2	84.0(5)	$O8^1$	Y1	O4	73.2(3)
O5	Y1	O2	132.5(3)	O3	Y1	O4	51.2(3)
$O4^1$	Y1	O2	147.0(3)	O2	Y1	O4	125.5(3)

O8[1]	Y1	O2	84.2(3)	O1	Y1	O4	117.6(3)
O3	Y1	O2	77.9(3)	O1	Y1	O4	117.6(3)
O6	Y1	O5	89.2(7)	O6	Y1	O1	76.5(5)
O6	Y1	O4[1]	80.1(4)	O5	Y1	O1	78.8(3)

Reference

1 H. Hao, Y. Wang, S. Yuan, D. Li and J. Sun, *Acta Crystallogr C Struct Chem*, 2018, **74**, 386-391.

2 H. Hao, H. Liu, Y. Wang, S. Yuan, H. Xu, J. Zhang, Y. Wang, D. Li and J. Sun, *Acta Crystallogr C Struct Chem*, 2019, **75**, 221-230.